Investigations into the Heterogeneity of Catalytically Active Sites of a Supported Organovanadium(III) Hydrogenation Catalyst via Computational Approaches

Prajay Patel, Robert Wells, David M. Kaphan, Massimiliano Delferro, Rex T. Skodje*, Cong Liu*

Corresponding emails: Rex.Skodje@colorado.edu, congliu@anl.gov

ABSTRACT

A crucial consideration for supported heterogeneous catalysts is the nonuniformity of the catalytic. With current spectroscopic techniques, populated sites of a catalytic system are measured as opposed to the catalytically active sites, which are often mutually exclusive. With computational models, often only a few representative structures are used to depict catalytic activity on a surface, even though numerous observable factors of surface heterogeneity play a role in the kinetically favorable active sites. To showcase the importance of modeling surface heterogeneity and its effect on catalytic activity, we apply density functional theory (DFT) computational models of a series of potential active sites for the reaction pathways, combined with kinetic Monte Carlo (kMC) simulations and compare those results to a previously reported experimental kinetic study of a surface organovanadium(III) catalyst [(SiO)V^{III}(Mes)(THF)] for styrene hydrogenation (Kaphan et al., ACS Catal., 2019, 9, 11055). DFT free energy reaction pathways indicated the likely active site and pathway for styrene hydrogenation; a heterolytic cleavage pathway requiring a bare tripodal vanadium site. From the kMC simulations, a mixture of the different bond lengths from the support oxygen to the metal center was required to qualitatively describe the experimentally observed kinetic aspects of a supported organovanadium(III) catalyst for olefin hydrogenation. This work exemplifies the importance of modeling surface heterogeneity in computational catalysis.

INTRODUCTION

Supported organometallic catalysts (SOMC) are used extensively to produce petrochemicals and fine chemicals due to their unique properties in combining the advantages of homogeneous and heterogeneous catalysis, selectivity and stability, respectively.[1-3] When modeling supported catalysts, the non-uniformity, or heterogeneity, of catalytically active sites (AS) is one of the more challenging aspects to depict. To this extent, the heterogeneity of AS has been understudied both experimentally and computationally since the overall observed activity is dominated by the catalytically most AS while standard spectroscopic techniques target the most populated sites.

Surface heterogeneity has been shown to have an effect on catalysis.[4] As an inherently kinetic process, modeling catalytic kinetics requires reliable mathematical models. Numerous kinetic studies are performed on defect-free surfaces through periodic density functional theory (DFT) and kinetic Monte Carlo (kMC) simulations. These models tend to follow simple Langmuir-Hinshelwood kinetics as a base assumption or the model and are simplistic for practical purposes. Through these assumptions, catalytic sites are modeled as energetically equivalent with equal reaction barriers. However, the observed complexity of catalytic kinetics and surface heterogeneity breaks these models, and while studies have examined defected or alloyed surfaces as well as stepped faces, a full scope of their effect on the kinetics is incomplete.

A common support for SOMC, amorphous silica surfaces (a-SiO_2) exhibit large degrees of heterogeneity in catalyst anchoring sites, which leads to an ensemble of catalytic sites with different structures and activities upon grafting of organometallic precursors.[5-6] Small variations, such as the bond distance and angle between a rigid silanol group and the metal atom, can lead to a normal distribution of reaction barriers during catalysis. Studies by Peters et al. illustrated a simplified model to calculate site-averaged grafting barriers of single atom catalysts on an a-SiO_2 surface that yielded a distribution of the kinetically favorable AS based on minor variations of the local environments of the grafting sites.[7-11] A study by Pucino et al. corroborates studying metal-surface interactions and surface heterogeneity for alkene metathesis tungsten catalysts as they found multiple tungsten sites on the silica surface with several different local environments.[12] These studies expand the need for more developed computational models and well-defined environments for describing surface heterogeneity in SOMC.

Amorphous silica based catalysts have been extensively studied with DFT methods,[13-15] in which two types of computational models have been commonly used for describing a-SiO_2, i.e., periodic slab models, which use a unit cell representation of the surface, and cluster models, a finite fragment of the solid. As amorphous surfaces have nonuniform composition and the need for more realistic and larger surface models increases, modeling amorphous supports with periodic slab models becomes increasingly challenging. On the other hand, computationally more efficient cluster and cage models have been utilized to study local AS environments of catalysts grafted onto amorphous silica. Previous computational studies in our group[15-16] as well as other studies[15-21] have shown that a cluster model of silica can well represent its bulk structures while keeping the surface strain on the cluster. Furthermore, silica clusters composed of different siloxane ring structures (silsequioxane) could be a good approximation of an a-SiO_2 surface.[17] Based on their success and previous use in our group to model SOMC, silsequioxane cages are utilized due to the number of structures needed for the full mechanistic nature of this investigation.

Kinetic Monte Carlo (kMC) applies Monte Carlo sampling towards catalytic chemistry through obtaining kinetic observables when the reaction environment plays a key role or when the reaction rates are non-uniform.[22-24] Using kMC and the single-molecule description of kinetics, we can explicitly view reaction profiles of each catalytic site to interpret bulk properties of the whole system, which is a composition of the turnovers from the individual sites. This work examines the impact of multi-step reaction pathways that contain correlations among their distributed energetic barriers on the production pathway for styrene hydrogenation.

Previous experimental work in our group developed the first hydrogenation-active supported organovanadium(III) site [$(SiO_2)V^{III}(Mes)(THF)$].[25] This catalyst is active for alkene hydrogenation and dehydrogenation of alkanes at both elevated and room temperature. Structure-property correlations revealed that low valent states and site isolation were required for hydrogenation. A follow-up experimental study by our group explored the mechanistic and kinetic profiles of this catalyst for styrene hydrogenation,[26] focusing on rate dependency on reactant concentration and possible inhibiting species. While experimental characterization and kinetic study provided structural insights and critical kinetic behaviors of [$(SiO_2)V^{III}(Mes)(THF)$], it is particularly meaningful to gain molecular understanding of the formation of the catalytically AS and the reaction mechanisms, as well as the role of the AS heterogeneity in the reaction energetics and observed kinetics.

Therefore, using the experimental findings as reference, two dimensions of AS heterogeneity are explored computationally in this work: 1) the surface heterogeneity based on bond elongation and coordination environment, and 2) considering the effects of various inhibitors to the catalytic activity, which allows the examination of a combination of potential AS rather than a single AS. Utilizing a multidimensional approach to model surface and AS heterogeneity leads to a derivation of site-averaged kinetics. The knowledge gained from this work could be adopted for future design of V(III) and other single-site metal catalysts on silica.

COMPUTATIONAL METHODS

Electronic Structure

All electronic structure calculations for the molecular structures and reaction energetics were performed using Gaussian16.[27] As shown in previous work, silsequioxane cages were shown to be adequate models for amorphous SiO_2 in lieu of periodic DFT calculations.[15] To model top monolayer relaxation in periodic models, the bottom half of the silica cluster (6 H, 11 O, and 6 Si atoms) was kept frozen during the optimization and frequency calculation. All structures were optimized using the B3LYP[28-29] density functional and CEP-31G[30-32] pseudopotential double-ζ basis set in the gas phase. For the free energy reaction profile, the Gibbs energy thermal corrections, single point energy, and frequency calculations are obtained using B3LYP with the TZVP[33] basis set at 50°C to replicate experimental conditions. The previous experiments used XXX as solvent, the effect of which was assumed to be small. Thus, solvents were not considered in these calculations.

Commented [PP1]: Dave: Which solvent was used in the experiments?

Kinetic Studies

Microkinetic and kinetic Monte Carlo (kMC) calculations are performed on the styrene hydrogenation network established via the DFT calculations in this work. The reaction

environment is simulated by creating approximately 1000 vanadium pre-catalysts in a solution of varying concentrations of styrene, H_2, and THF molecules. The THF to catalyst ratio stays at a minimal 1:1 ratio due to the observed kinetics of THF as an inhibitor in previous work. Each catalyst site is treated as rigid so that energetic barriers are categorized by V-O bond distance. An equilibrium approximation was used for species that undergo rapid interconversion. (DETAILED INFORMATION ABOUT SOFTWARE)

Commented [PP2]: Rob/Rex: Please provide information about the software used for kMC simulations.

RESULTS AND DISCUSSION

1. Computational models of catalytic sites considering surface heterogeneity

The investigation begins with a set of pre-catalyst structures formed after grafting. The experimental grafting reaction undergoes the metalation of partially dehydroxylated amorphous silica with the molecular organometallic precursor ([$V(Mes)_3(THF)$]).[25] Upon the formation of the supported pre-catalyst, the previous nuclear magnetic resonance (NMR)-scale vanadation experiments showed the release of two out of three mesitylene groups and negligible THF from the original molecular precursor. As well, the X-ray Absorption Near-Edge Structure (XANES) spectra showed a 3+ oxidation state for the V center.[26] Based on these observations, we propose three different pre-catalyst structures formed from three distinct grafting sites on silica (Figure 1): a four-coordinate bipodal site (**1**), a tripodal site with a silanol donor (**1b**), and a tripodal site with a siloxane donor (**1c**). In all three sites, the V center is bound to a THF and a mesitylene, and each of these sites represent the scenario where the molecular precursor is grafted onto a unique coordination site on amorphous silica. In the Section 2 on the formation of catalytically AS, we will mainly focus on comparison among different coordination sites (i.e., **1**, **1b** and **1c**). In addition to the coordination environment, we found that the local geometric parameters of the surface donor species could play an important role in the catalytic reactions, e.g., the siloxane donor of **1c**. Thus, in the catalytic hydrogenation subsection, we will discuss how the V-O(siloxane) distance in **1c** affects the reaction energetics.

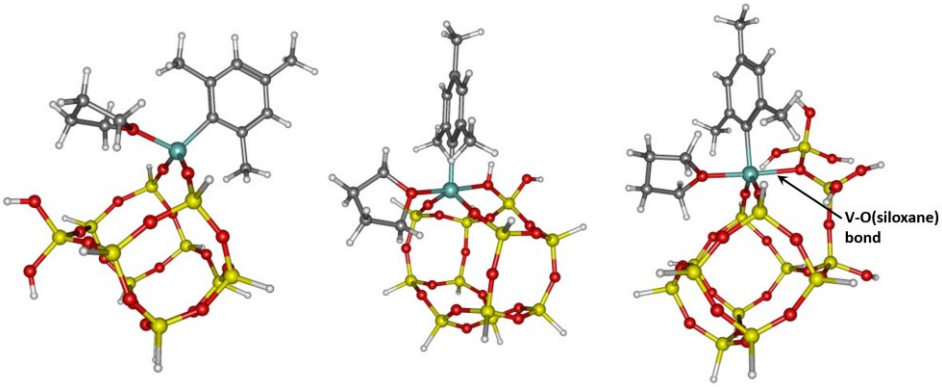

Figure 1. Cluster models of proposed pre-catalyst structures **1** (left), **1b** (middle) and **1c** (right).

For the cluster models of **1** and **1b**, we allow the top half of the silica cluster to relax while keeping the bottom half (6 H, 11 O, and 6 Si) frozen during geometry optimization. However, for

1c, the two Si-O groups and the bottom half of the silica cluster are treated the same as for **1** and **1b** while for the siloxane donor (Si-O-Si), we consider two scenarios to represent the heterogeneity of the local geometries of grafted catalysts with the siloxane donor. The first scenario utilizes the rigidness of the neutral siloxane groups on the surface of amorphous silica, which infers the positions of the siloxane relative to the metal center are not likely to change during grafting and catalysis. Here we use the V-O(siloxane) distance as a parameter for a simplified description of the siloxane position relative to the metal center. Although other geometric parameters, such as bond angles and dihedrals, as well as the distance between two ≡SiO− groups, could also play a role in describing the relative position of the siloxane, we found the V-O (siloxane) distance is an effective simplification that is sufficient to demonstrate a qualitative trend in catalysis (See Sections 2 and 3). Based on the optimal V-O (siloxane) distance for **1c** (2.29 Å) in the FTM model, we consider three rigid V-O (siloxane) distances: *2.1*, *2.3* and *2.5* Å. In all calculations, the V-O distance is kept constant while the other geometric parameters are optimized. An alternative scenario considers the small chance of proximity between the donor siloxane and the edge or corner of the amorphous silica sample, which could provide more flexibility for the siloxane donor during grafting and catalysis given the extra degrees of freedom. In this case and for fundamental comparison with the first scenario, we also consider a system where the siloxane is unconstrained and therefore can fully relax, denoted as "*free to move (FTM)*", during geometry optimization. As a result, we have six total proposed pre-catalyst systems, including **1**, **1b**, and **1c** for each individual V-O(siloxane) distance, i.e. FTM, 2.1, 2.3, and 2.5 Å (Figure 1).

2. Formation of catalytically active sites

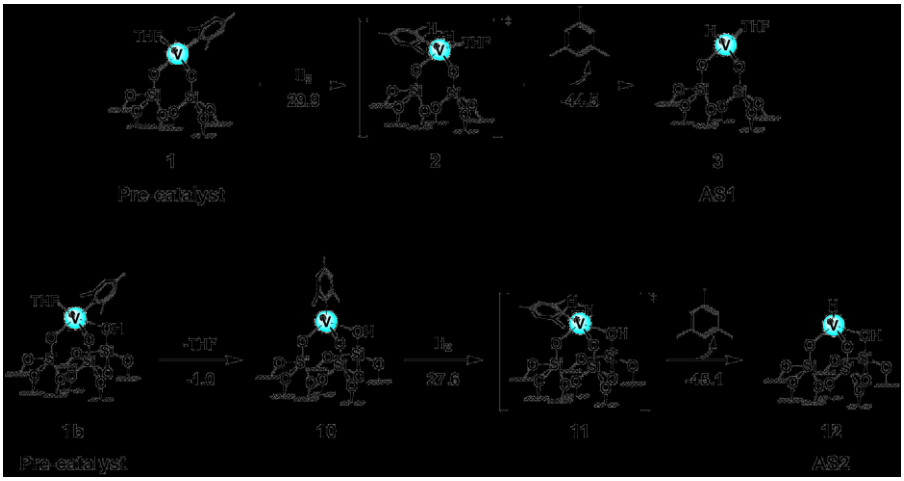

Scheme 1. Proposed reaction pathways of the formation of potential AS1 (**3**) and AS2 (**12**) for styrene hydrogenation. All free energies are reported in kcal/mol.

Our previous experiments discovered that interaction of the pre-catalyst with H_2 activates the catalyst and forms a catalytically AS that catalyzes styrene hydrogenation and regenerates after

the catalytic cycle. X-ray Absorption Near-Edge Structure (XANES) and Extended X-ray Absorption Fine Structure (EXAFS) spectra showed that treating the pre-catalyst with H_2 leads to a reduction of the coordination number of non-hydrogen ligands with THF present on the surface and the vanadium center remaining an 3+ oxidation state.[26] Solely based on this characterization, it is uncertain whether the AS formed from the pre-catalyst is a lower-coordinate V site or a V-H site because the hydride is not observable in EXAFS. It is also unclear whether all the THF ligands remain on the metal center after H_2 treatment. Therefore, we consider all these possible structures along with their associated reaction pathways for the six proposed pre-catalyst structures. The initial interactions of **1** and **1b** (Scheme 1) and **1c** (Scheme 2) with H_2 undergoes σ-bond metathesis of the mesitylene ligand. Our preliminary calculations (See SI for details) show that the four-coordinate V site (**1**) energetically prefers the presence of THF ligand during metathesis, while the five-coordinate V sites (**1b** and **1c**) sterically requires the dissociation of THF before metathesis. **1** and **1b** form V-H species **3** ($\Delta G^{\ddagger}_{intrinsic}$ = 29.9 kcal/mol) and **12** ($\Delta G^{\ddagger}_{intrinsic}$ = 28.6 kcal/mol), respectively, which are identified to be their catalytically AS, respectively (for the continued catalytic cycles, see Scheme 3). On the other hand, **1c** first undergoes σ-bond metathesis to form a V-H (**3c** without THF or **3b** with THF) that can continue to react with the coordinated siloxane group on the support, resulting in a Si-H and a tripodal bare V site either with or without THF (**25** without THF or **25b** with THF). Such a hydride transfer reaction has been reported previously for a silica supported Zr-H, in which Si-H was observed via nuclear magnetic resonance (NMR) spectroscopy.[34] Here we consider the four structures for **1c** described earlier. As shown in Scheme 2, although the intrinsic barrier of the σ-bond metathesis (**10b** → **3c**) decreases (from 27.1 to 22.0 kcal/mol) with the increase of the V-O(siloxane) distance, all the systems show a very similar apparent barrier (18.6-19.1 kcal/mol). The hydride transfer reaction (**3b** → **25** or **3c** → **25b**) shows very low barriers (≤ 6.7 kcal/mol) in all cases. This indicates the hydrides (either **3b** or **3c**) resulting from the σ-bond metathesis are likely to have a very short lifetime and quickly transform to either a bare V tripodal site (**25b**) or a THF bound V site (**25**). It is notable that the apparent barrier of **1c** activation reaction is much lower than those of pre-catalysts **1** and **1b** (29.9 and 27.6 kcal/mol, respectively), and the highest intrinsic barrier (27.1 kcal/mol at V-O(siloxane) = 2.1 Å) among the considered **1c** structures is also lower than those of **1** and **1b**. This indicates that the activation of **1c** by H_2 could be kinetically more favorable in general than **1** and **1b**.

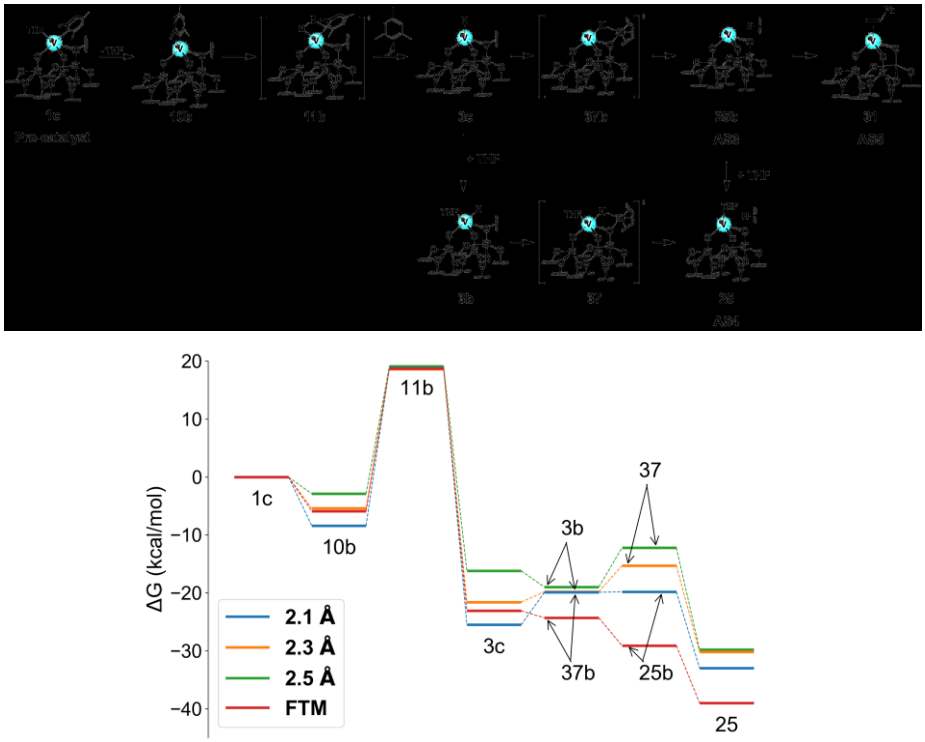

Scheme 2. (top) Proposed reaction pathways of the formation of active sites 3 (**25b**) and 4 (**25**) for styrene hydrogenation. (bottom) The lowest free energy pathways for the formation of **25** and **25b** as a function of the V-O(siloxane) distance. The reaction free energies of higher energy pathways see Table S1.

It is also notable that THF binds onto or dissociates from the V site at different reaction steps depending on the reaction energetics. σ-bond metathesis (**10b** → **3c**) occurs after the dissociation of THF (**1c** → **10b**) for all V-O(siloxane) distances. However, for the hydride transfer reaction, sites with shorter V-O(siloxane) distances (2.1 and FTM) energetically favor the pathway without THF (**3c** → **37b** → **25b**), while those with longer V-O(siloxane) distances (2.3 and 2.5 Å) undergoes the pathway with THF (**3c** → **3b** → **37** → **25**). This demonstrates the dynamic behavior of the THF coordination during the formation of individual catalytic sites. Although the resulting THF coordinated V site (**25**) is thermodynamically more stable than the bare V site (**25b**) in all cases, we hypothesize that both sites could exist under the reported experimental condition[26] and potentially be the AS, due to the low concentration of THF (dissociated from the initial molecular precursor) in the experiment. In addition to AS3 and AS4, we also hypothesize that styrene, which presents a much higher concentration (286 times higher) than THF in the experiment, could also act as a binding substrate to the bare V site in AS3 (**25b**), forming a potential AS5 (**31**) (Scheme 2). Further analysis on the stability of the AS and their potential roles in catalytic hydrogenation

is presented in later subsections. Both the reaction pathways and energetics of the AS formation are affected by the V-O(siloxane) distance, and so we anticipate that the V-O(siloxane) distance could also be critical to the catalytic hydrogenation of styrene.

3. Catalytic Hydrogenation

Active Sites 1 and 2. Scheme 3 outlines the proposed catalytic cycles for styrene hydrogenation with AS1 (**3)** and AS2 (**12)**, which are generated from activation of **1** and **1b** by H_2, respectively. These two systems will be discussed together because they share a similar catalytic reaction mechanism. The reaction pathway of AS1 (**3**) undergoes hydride insertion (**3** → **8**) into the secondary carbon of styrene forming a V-alkyl **8** with a 22.5 kcal/mol barrier. An alternative pathway where the V center forms a bond with the secondary carbon of styrene yielded a slightly higher barrier (22.7 kcal/mol) (Figure S1). From intermediate **8**, an additional H_2 was required for the hydrogenolysis of the alkyl (**8** → **3**) and regenerate AS1 (**3**). In the case of AS2 (**12**), the hydride insertion (**12** → **17**) into the primary carbon of styrene results in **17** via a 35.7 kcal/mol barrier, and the hydrogenolysis of **17** (**17** → **12**) with a 34.5 kcal/mol barrier regenerates AS2 (**12**). (Alternative pathway see Figure S1).

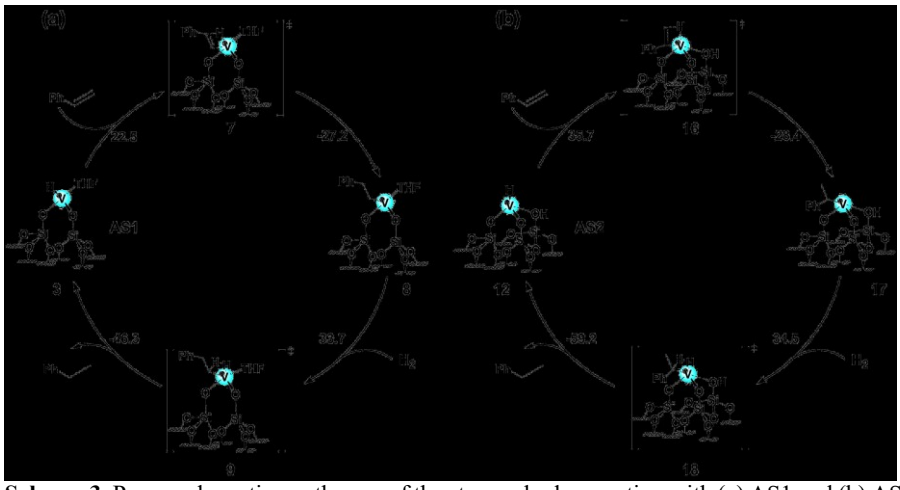

Scheme 3. Proposed reaction pathways of the styrene hydrogenation with (a) AS1 and (b) AS2. All free energies are reported in kcal/mol.

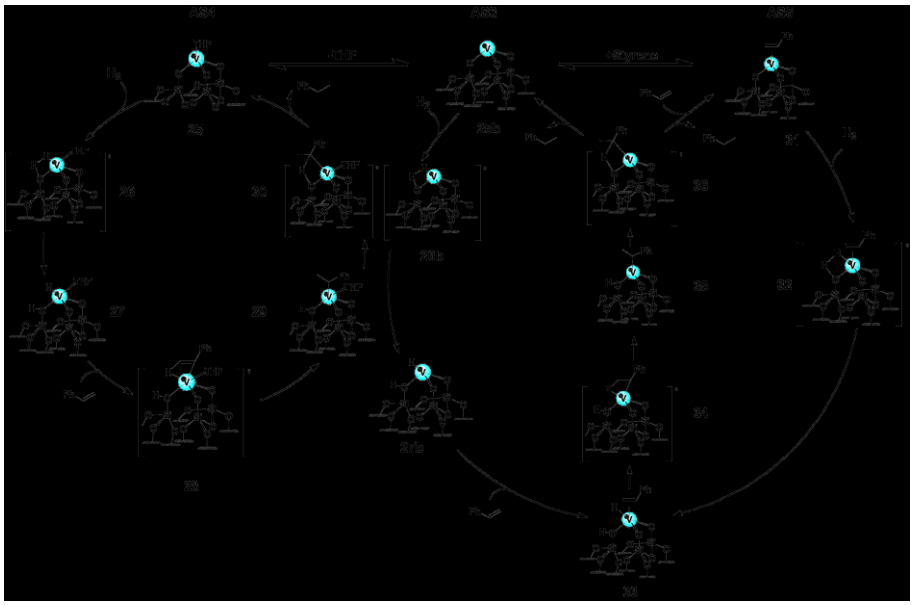

Scheme 4. Proposed styrene hydrogenation pathways for modeling AS heterogeneity from AS3, AS4 and AS5.

Active Sites 3, 4, and 5. Scheme 4 shows the proposed reaction network for styrene hydrogenation catalyzed by AS3, AS4 and AS5. While individual reaction steps and intermediate structures vary depending on the AS structure, all three AS follow a similar catalytic mechanism: heterolytic cleavage of H_2 followed by step-wised hydrogen transfer to styrene. Since AS3 and AS5 share the same pathway for the hydrogen transfer to styrene (**33** → **36**), they are herein discussed together. As shown in Figure 2a and 2c, we see a general trend of the reaction free energies as a function of V-O(siloxane) distance: the longer the V-O(siloxane) distance, the lower the pathway is lying in the reaction energy diagram. The FTM model shows the highest energy reaction pathway among all the models, presumably because its pre-catalyst activation undergoes the most exergonic reaction resulting in a relatively more stable (less active) active site than the three other model systems. For both AS3 and AS5, as the V-O(siloxane) distance increases from 2.1 to 2.5 Å, the H_2 cleavage barriers (**25b** → **26b** and **31** → **32**) decrease except for **25b** → **26b** at 2.3 and 2.5 Å, and

forms more stable intermediates relative to the AS. While the reaction barriers of the hydride insertion to styrene (**33** → **34**) are not affected by the V-O(siloxane) distance remarkably, those of the 1,2-elimination (**35** → **36**) increase dramatically as the V-O(siloxane) distance increases, likely due to the stabilization of the V-alkyl intermediate (**35**). Eventually at V-O(siloxane) = 2.5 Å, the V-alkyl intermediate becomes the thermodynamically most stable state in the catalytic pathway, and we observed comparable barriers from **35** going forward (1,2-elimination, **35** → **36**, 25.25

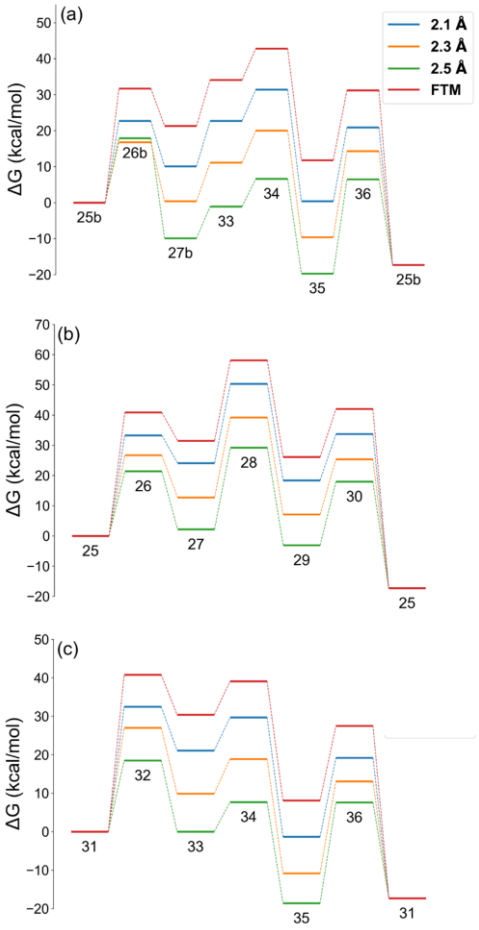

Figure 2. Free energy diagrams for the styrene hydrogenation with (a) AS3 (b) AS4, and (c) AS5. The V-O(siloxane) distances are represented by lines (2.1 - blue, 2.3 - orange, 2.5 - green, and free to move - red). All free energies are reported in kcal/mol.

kcal/mol) and going backward (β-hydride elimination, **35** → **34**, 25.28 kcal/mol). This indicates that at longer V-O(siloxane) distances, the alkyl intermediate could act as a kinetic resting state, from which the reactions going forward and backward become reversible. The importance of this observation and its relevance to the experimental study will be discussed in the Section 3. The similarity between the pathways of AS3 and AS5 also presents in the changing trend of the rate-limiting step (RLS); as the V-O(siloxane) distance increases, the RLS switches from the heterolytic H_2 cleavage to the 1,2-elimination step. The switching occurs at 2.3 Å for AS3, and at 2.5 Å for AS5. To note, the barrier heights of the heterolytic H_2 cleavage is always lower for AS3 than for AS5 at each individual V-O(siloxane) distance. This indicates that styrene is acting as an inhibitor to the catalyst. Especially for catalytic systems with shorter V-O(siloxane) distances, where the RLS is the heterolytic H_2 cleavage, AS3 is likely to be kinetically more favorable than AS5.

On the other hand, the catalytic pathway of AS4 (Figure 2b) shows similar energetic trends to those of AS3 and AS5. However, the barrier heights and relative energies of the intermediates of AS4 are all higher than those of the other two sites at each individual V-O(siloxane) distance. What is also different is the RLS; it switches from the heterolytic H_2 cleavage (**25** → **27**) to the hydride insertion (**27** → **29**) as the V-O(siloxane) distance increases to 2.5 Å, at which the reversibility between the 1,2-elimination (**29** → **30**) and β-hydride elimination (**29** → **28**) from the V-alkyl (**29**) is still not reached. These results suggest that THF also acts as an inhibitor to the catalyst, and the catalytic pathways of the THF bound AS4 are not as energetically favorable as AS3 and AS5.

It is worth noting that the reaction barrier of heterolytic H_2 cleavage decreases as the V-O distance increases in general. This indicates among the three V-O bonds of a tripodal V site (AS3), H_2 cleavage could likely occur on the longest V-O bond. Here the V-O(siloxane) bond varies from 2.1 to 2.5 Å, longer than the other two V-O bonds (around 1.98 Å). Thus, in the considered models, it is reasonable to assume the H_2 cleavage occurs on the V-O(siloxane) bond. Additional calculations (Table S5) were carried out by varying the O-O distance of the other two V-O bonds. The results show that when the V-O(siloxane) bond is set at 2.1 Å, the H_2 cleavage barriers showed an opposite trend as a function of the O-O distance compared to those as a function of the V-O(siloxane) distance. This demonstrates another dimension of the site heterogeneity. Knowing the incompleteness of the current models, which did not consider the distribution of the other two V-O bond lengths, we will focus on a qualitative analysis for the following kinetic modeling (Section 6).

For all the respective pathways in Figure 2, the fully relaxed model (FTM), which could represent catalytic sites on the surface edges with more labile siloxane donors, yielded the highest reaction barriers. This indicates that the hydrogenation catalysis is not favorable to react on the catalytic sites on the edge of silica support. Thus, in the following sections FTM was omitted from the discussions.

4. Stability among Active Sites and Intermediate States

The relative stability among AS3 through AS5 is measured by the reaction free energies (ΔG) of the conversion among the three sites; higher ΔG yields a lower relative stability. The conversion of AS3 to AS4 and AS5 results from the adsorption of THF and styrene, respectively. We hypothesize that when the reaction free energy of adsorption/desorption of THF or styrene is

small (a few kcal/mol) the relative stability between two AS becomes near-equilibrium, and the conversion between the two could be facile. Such conversion reflects the dynamic change possibly occurring on a catalytically AS during catalysis. Figure 3 shows the calculated relative stability among the three AS (Figure 3a) and that among the corresponding hydrides (Figure 3b) as a function of the V-O(siloxane) distance. As shown in Figure 3a, the relative stability of each active site decreases as the V-O(siloxane) distance increases, indicating the AS at longer V-O(siloxane) distances tend to be more reactive. This is consistent with the trends of the calculated reaction pathways, where lower barriers correspond to increasing the V-O(siloxane) distance. On the other hand, for each individual V-O(siloxane) distance, AS3 and AS5 tend to have very similar stability while AS4 (THF coordinated V site) is much more stable thermodynamically (by 13.2−16.5 kcal/mol) than AS3 and AS5. The similar stability between AS3 and AS5 suggests that the binding of a styrene onto a bare V site is not particularly favorable. In other words, although styrene presents a high concentration in the experimental condition, it is not likely to become a strong inhibitor to the catalytic reaction. However, the much higher stability of THF coordinated AS4 suggests that THF could become problematic to the catalytic reaction at high THF concentrations; the bare V sites (AS3) are likely to bind with THF prior to interacting with H_2, leading to higher H_2 cleavage barriers. Nevertheless, once the hydride intermediates (**27b**, **27** and **33**) are formed, the order of the stability changes (Figure 3b). The styrene coordinated hydride (**33**) becomes less stable, and the difference in stability between the bare V-H and the THF coordinated hydride becomes minor (≤ 3.8 kcal/mol). This indicates that once the hydride is formed, THF could dynamically desorb from the V site, leading to much smaller barriers in the following catalytic pathway (Figure 2). At low THF concentrations, most AS are likely to be the bare V sites, which would have more impact on the overall kinetics in the catalytic reaction.

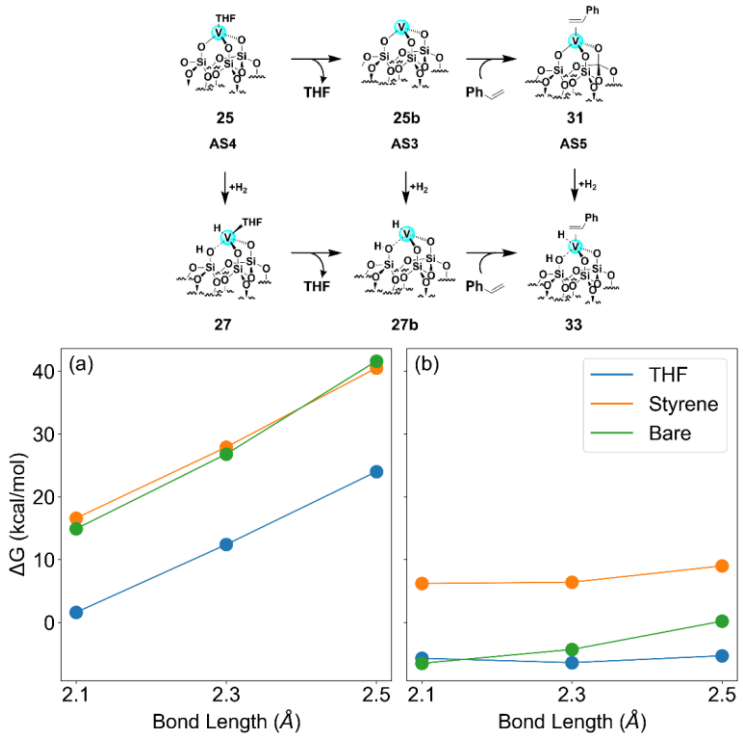

Figure 3. The relative stability of(a) AS and (b) their hydrides (b). THF – blue, styrene – orange, bare V site – green.

5. Correlation with Experimental Mechanistic Study

Commented [PP3]: Max/Dave: Please provide input on this section.

The direct correlations between the previous experimental investigations and the present computational studies of the AS and mechanisms are summarized in Table 1. In general, the structures of all the proposed pre-catalysts and AS are consistent with the experimental characterization. However, the reaction mechanisms of AS1 and AS2 were found to have major inconsistency with the deuterium incorporation experiments. The deuterium incorporation under various D_2 pressures showed that varying the D_2 pressure does not change the ratio of deuterium incorporated between the primary and secondary carbon atoms in styrene. This suggests that the hydrogenolysis of the V-alkyl and the β-hydride elimination step would have the same order with regard to hydrogen.[26] AS1 and AS2 both require an additional H_2 in the hydrogenolysis step (Steps **8** → **3** and **17** → **12**, respectively, Scheme 3) , which leads to a different order of reaction compared to the hydrogenolysis step (Steps **3** → **8** and **12** → **17**, respectively, Scheme 3). This eliminates AS1 and AS2 from the list of potential AS. The reaction mechanism of AS3-AS5, on the other hand, has the same order for both steps, consistent with experiments. Furthermore, active site NMR experiments during deuteration shows that the signal of protons in the primary carbon of the styrene diminished more rapidly than the signals associated with the proton at the secondary carbon or those associated with the aromatic ring, suggesting that at least some of deuterium was

incorporated into the starting styrene by *reversible* hydride insertion. This would require the reaction barrier of the hydrogen transfer (barrier A) to the alkyl intermediate to be comparable or higher than that of the β-hydride elimination from the alkyl intermediate back to V-H and styrene (barrier B). These two reaction barriers refer to steps **35** → **36** (barrier A) and **35** → **34** (barrier B) for AS3 and AS5, and steps **29** → **30** (barrier A) and **29** → **28** (barrier B) for AS4 (Scheme 4). In Figure 2, the calculations show a general trend between these two barriers as a function of the V-O(siloxane) distance. As the V-O(siloxane) distance increases, barrier A increases while barrier B decreases. And at V-O(siloxane) = 2.5 Å, barrier B (26.2 kcal/mol) becomes comparable with barrier A (26.3 kcal/mol) for AS3 and AS5, indicating the sites with longer V-O(siloxane) distances could have a reversible hydride insertion. These computational results support the observed reversible hydride insertion, and further emphasize the importance to consider site heterogeneity.

Table 1. Summary of computational relevance to the experimental mechanistic study. "Y" denotes that the computational results are consistent with experiments, while "N" denotes an inconsistency.

Pre-catalyst		**1**	**1b**	**1c**		
Exp. characterization (NMR)[25-26]	4- or 5-coordinate with both THF and Mes ligands	Y	Y	Y		
Active Site (AS)		1	2	3	4	5
Exp. characterization (XAS)[25-26]	Reduction of coordination number of non-hydrogen ligands after H_2 treatment	Y	Y	Y	Y	Y
Exp. Mechanistic Study[26]	Deuterium incorporation pressure dependence	N	N	Y	Y	Y
	Reversible hydride insertion	-	-	2.5 Å	-	2.5 Å

These correlations with experiment eliminate AS1 and AS2 from the list of potential AS. Among AS3-AS5, the calculated relative stability, as discussed in the previous subsection (Figure 3), shows that styrene binding onto either the AS3 (to form AS5) or the hydride intermediate does not increase the stability of the sites and leads to higher reaction barriers, indicating styrene is a poor inhibitor. Thus, in the following subsection, reaction pathways of AS3 and AS5, as well as the possible reversible conversion between these two AS were considered for kinetic Monte Carlo simulations to illustrate the kinetic dependency of styrene, H_2 pressure, and THF.

6. Kinetic Monte Carlo Simulations of Rate Dependence

Kinetic Monte Carlo (kMC) simulations were carried out to reproduce the experimental kinetic results and to validate the importance of the site heterogeneity. The kMC simulation results were focused on the experimental kinetic dependency of styrene, H_2 pressure, and THF,[26] rather than quantitative agreement of the production rates. These simulations take into account the effect of V-O(siloxane) distance, integrating both perspectives of surface heterogeneity and inhibiting species.

Figure 4a-c shows the experimental kinetic dependency of styrene, H_2 pressure, and THF.[26] The previous kinetic study[26] found a nonlinear dependence of the styrene concentration and hydrogen pressure on the production rates. The styrene dependence closely resembles a Michaelis-Menten like hyper bolic dependence. The hydrogen dependence, while not the pronounced hyperbolic dependence of styrene, is still highly non-linear.

The transition rate between two states is given by the pseudo-first order rate coefficient $k(T) = \frac{kT}{h} \cdot \chi \cdot \exp(-\frac{\triangle G_0^{\ddagger}}{kT})$ where $\triangle G_0^{\ddagger}$ is the free energy barrier and χ represents the concentration of a co-reagent, such as H_2. An equilibrium approximation within the kMC was used for species that undergo rapid interconversion. The species in equilibrium are AS3 and AS4 (**25b** and **25**) as well as their hydrides (**27b** and **27**). Here we recall that AS4 (**25**) is thermodynamically more stable than AS3 (**25b**), but the energy difference between the two hydrides are small ($\leq$ 3.8 kcal/mol) (Figure 3). We first examined the dependence of styrene concentration on the production rate across the three V-O(siloxane) distances (2.1, 2.3 and 2.5 Å). kMC simulations of the FTM model is not discussed here as it consistently showed the lowest rate of all scenarios (Details Tables S6, S7 and S8). Styrene hydrogenation occurs in a concerted fashion with styrene binding on the two pathways. Figure 4d shows the simulated styrene dependency between 0.01 ML to 3.0 ML. Production rates vary by orders of magnitude among the three V-O(siloxane) distances. The 2.3 Å model has the fastest production rate and shows the most qualitatively consistent concentration dependence with experiment (Figure 4a). It also is the data set which contains the highest amount of AS3 (greater than 5%).

For the H_2 dependence, there are noticeable similarities to styrene. The production rate was still the highest for the 2.3 Å model with no apparent H_2 dependence; however, H_2 exhibited a greater dependence on the rate of product formation, which ranges over two orders of magnitude for the 2.1 Å model (Figure 4e). For this dependence to be exhibited in a simulation where the distributions of rate are present, the selectivity of the 2.3 Å pathway must be larger than that of the 2.1 Å pathway by a sizable amount. This indicates the number of the 2.1 Å AS is much bigger than that of the 2.1 Å AS. Both the styrene and H_2 substrates will only have effects on the production rate and that their concentrations are irrelevant to the production pathways. Examining the 2.1 Å result for H_2 production rates, the rate dependence does not plateau, which agrees qualitatively with the experimental H_2 pressure dependence.

The relationship between THF concentration and production rate is the most complex of all three binding species. Experimentally, THF acts as an inhibitor; increasing the concentration of THF decreases the production rate. As illustrated earlier, THF as the inhibitor was proposed due to the high stability of AS4 **(25)** relative to AS3 and AS5 (**31** and **25b**) (Figure 3a). However, the near-equilibrium between the THF coordinated hydride (**27**) and the bare hydride (**27b**) (Figure 3b) indicates that THF could become bound and unbound multiple times during the reaction pathway. Such complexity was clearly reflected in the rate dependence of THF. The 2.3 Å model yielded the highest amount of production for the pathway of AS4. A slight inhibition effect is observed for the 2.1 Å model (Figure 4f). However, the opposite correlation was observed for both the 2.3 Å and 2.5 Å models; increasing the THF concentration increased the production rate. Also, the THF concentration is directly correlated with a decrease in production via **27b** and an increase in production via **27**. Overall, with both the 2.1 Å and 2.3 Å models in parts showing qualitatively consistent kinetic profiles with experiment indicates that there is a dynamic distribution of contributions from different AS structures to the overall observed reaction rate for styrene hydrogenation.

When using a linear combination of the simulated kinetic profiles for each V-O distance (Figure 4g-i), the production rate profiles qualitatively aligns with the experimentally observed kinetics. This was achieved with a linear combination of 92% of the 2.1 Å model with 4% of the 2.3 Å and 2.5 Å models each. Therefore, to properly describe reaction kinetics of styrene hydrogenation with the present computational models, a distribution of different V-O(siloxane) bond lengths was required. Note that the kMC results using the current models are meaningful in the qualitative fashion, demonstrating an effective strategy and highlighting the importance to consider AS heterogeneity in studying catalytic reaction mechanisms for SOMC. With improved and more complete computational models of AS, these quantitative numbers of the AS distribution could vary.

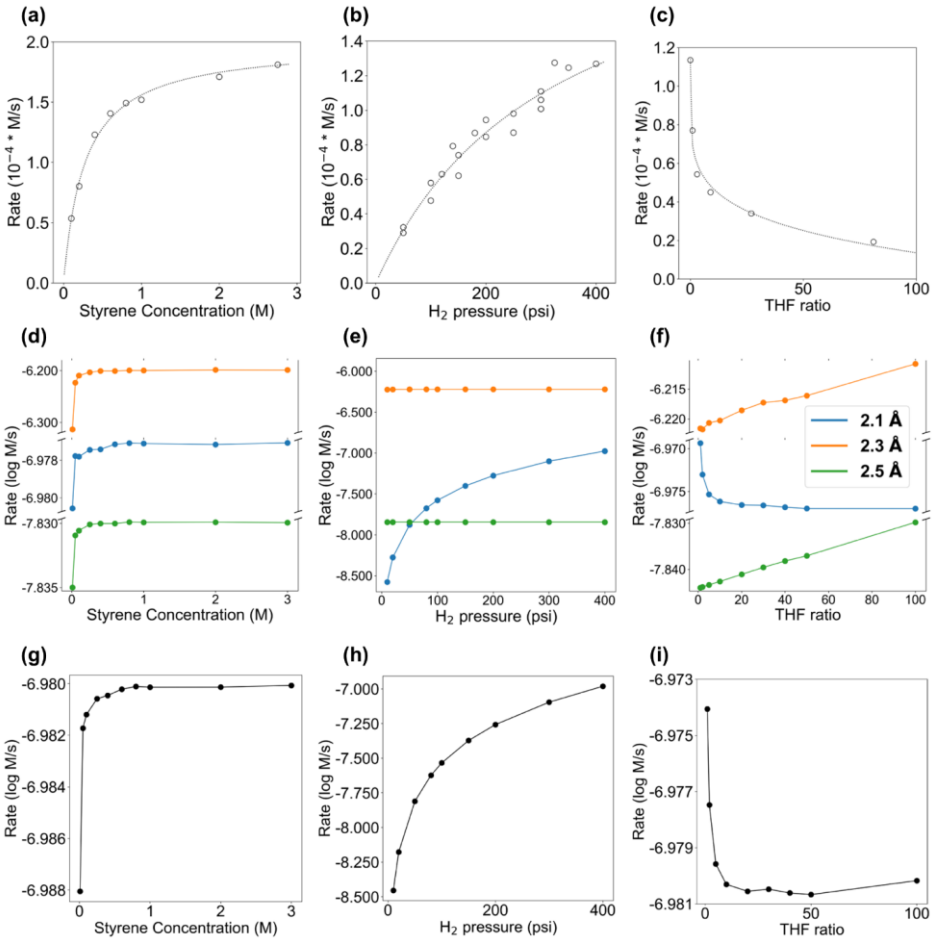

Figure 4. Experimental kinetic dependencies on (a) styrene, (b) H_2 pressure, and (c) the ratio of THF for styrene hydrogenation. Kinetic Monte Carlo (kMC) calculated kinetic dependencies on (d) styrene, (e) H_2 pressure, and (f) THF ratio at V-O(siloxane) = 2.1 (blue), 2.3 (orange), and 2.5 (green) Å. kMC calculated kinetic dependencies on (g) styrene, (h) H_2 pressure, and (i) THF ratio using a linear combination of 92% 2.1, 4% 2.3, and 4% 2.5 Å.

CONCLUSIONS

Overall, this work showcases investigating active site heterogeneity through a multidimensional computational approach. The reaction pathways computed via DFT showed the identified more likely AS, among which the calculated relative stability provides critical insights to the dynamic conversion among different sites during catalysis. For styrene hydrogenation, this pertains to the behavior of THF as an inhibitor and reactivity of the catalyst post-H_2 treatment. The DFT pathways supported the experimentally observed kinetics in that THF was a poor inhibitor given the high activation barrier. The proposed mechanism for styrene hydrogenation follows the heterolytic cleavage mechanism with H_2 acting as the inhibitor in the most energetically favorable pathway. From the dimension of surface heterogeneity, the fully relaxed model is not necessarily a valid model to represent all the AS based on both DFT and kinetic analysis. The kinetic Monte Carlo simulations of varying reactant concentrations indicated that using both V-O(siloxane) bond lengths of 2.1 Å and 2.3 Å for the catalyst models were required to gain a full qualitative understanding of the reaction kinetics.

From both the DFT and kMC perspectives, the qualitative accuracy with respect to the previous experimental work illustrates the importance of modeling surface heterogeneity when developing theoretical approaches to understanding single site heterogeneous catalysts. Yet to gain quantitative accuracy for catalytic kinetics, more rigorous computational models of SOMC are to be developed.

SUPPORTING INFORMATION

XYZ files for all the catalyst structures used for the reaction pathways. Additional schematics of reaction pathways.

ACKNOWLEDGEMENTS

This work was supported by the U.S. Department of Energy (DOE) Office of Basic Energy Sciences, Division of Chemical Sciences, Geosciences, and Biosciences, under Contract DE-AC02-06CH11357 (Argonne National Laboratory). All DFT calculations were performed using the computational resources at provided by the Laboratory Computing Resource Center (LCRC) at Argonne National Laboratory (ANL).

Grant numbers for Rex's group

REFERENCES

1. Lefebvre, F.; Basset, J. M., Recent applications in catalysis of surface organometallic chemistry. *J Mol Catal a-Chem* **1999,** *146* (1-2), 3-12.
2. Pelletier, J. D.; Basset, J. M., Catalysis by Design: Well-Defined Single-Site Heterogeneous Catalysts. *Accounts of Chemical Research* **2016,** *49* (4), 664-77.
3. Samantaray, M. K.; Pump, E.; Bendjeriou-Sedjerari, A.; D'Elia, V.; Pelletier, J. D. A.; Guidotti, M.; Psaro, R.; Basset, J. M., Surface organometallic chemistry in heterogeneous catalysis. *Chemical Society Reviews* **2018,** *47* (22), 8403-8437.
4. Murzin, D. Y., On Surface Heterogeneity and Catalytic Kinetics. *Industrial & Engineering Chemistry Research* **2005,** *44* (6), 1688-1697.
5. Thomas, J. M.; Raja, R.; Lewis, D. W., Single-Site Heterogeneous Catalysts. *Angewandte Chemie International Edition* **2005,** *44* (40), 6456-6482.
6. Gajan, D.; Copéret, C., Silica-supported single-site catalysts: to be or not to be? A conjecture on silica surfaces. *New Journal of Chemistry* **2011,** *35* (11).
7. Peters, B.; Scott, S. L., Single atom catalysts on amorphous supports: A quenched disorder perspective. *Journal of Chemical Physics* **2015,** *142* (10), 104708.
8. Goldsmith, B. R.; Peters, B.; Johnson, J. K.; Gates, B. C.; Scott, S. L., Beyond Ordered Materials: Understanding Catalytic Sites on Amorphous Solids. *ACS Catal* **2017,** *7* (11), 7543-7557.
9. Peters, B., Catalysis. In *Reaction Rate Theory and Rare Events Simulations*, Peters, B., Ed. Elsevier: Amsterdam, 2017; pp 79-128.
10. Khan, S. A.; Vandervelden, C. A.; Scott, S. L.; Peters, B., Grafting metal complexes onto amorphous supports: from elementary steps to catalyst site populations via kernel regression. *React Chem Eng* **2020,** *5* (1), 66-76.
11. Vandervelden, C. A.; Khan, S. A.; Scott, S. L.; Peters, B., Site-averaged kinetics for catalysts on amorphous supports: an importance learning algorithm. *React Chem Eng* **2020,** *5* (1), 77-86.
12. Pucino, M.; Liao, W. C.; Chan, K. W.; Lam, E.; Schowner, R.; Zhizhko, P. A.; Buchmeiser, M. R.; Copéret, C., Metal-Surface Interactions and Surface Heterogeneity in 'Well-Defined' Silica-Supported Alkene Metathesis Catalysts: Evidences and Consequences. *Helvetica Chimica Acta* **2020,** *103* (6).
13. Islam, M. M.; Costa, D.; Calatayud, M.; Tielens, F., Characterization of Supported Vanadium Oxide Species on Silica: A Periodic DFT Investigation. *The Journal of Physical Chemistry C* **2009,** *113* (24), 10740-10746.
14. Tielens, F.; Gierada, M.; Handzlik, J.; Calatayud, M., Characterization of amorphous silica based catalysts using DFT computational methods. *Catalysis Today* **2020,** *354*, 3-18.
15. Liu, C.; Camacho-Bunquin, J.; Ferrandon, M.; Savara, A.; Sohn, H.; Yang, D.; Kaphan, D. M.; Langeslay, R. R.; Ignacio-de Leon, P. A.; Liu, S.; Das, U.; Yang, B.; Hock, A. S.; Stair, P. C.; Curtiss, L. A.; Delferro, M., Development of activity–descriptor relationships for supported metal ion hydrogenation catalysts on silica. *Polyhedron* **2018,** *152*, 73-83.
16. Plascencia, C.; Curtiss, L. A.; Liu, C., Hydrogen Activation by Silica-Supported Metal Ion Catalysts: Catalytic Properties of Metals and Performance of DFT Functionals. *Journal of Physical Chemistry A* **2019,** *123* (1), 171-186.
17. Feher, F. J.; Newman, D. A.; Walzer, J. F., Silsesquioxanes as models for silica surfaces. *Journal of the American Chemical Society* **1989,** *111* (5), 1741-1748.

18. Fraile, J. M.; Garcia, J. I.; Mayoral, J. A.; Vispe, E., Catalytic sites in silica-supported titanium catalysts: silsesquioxane complexes as models. *Journal of Catalysis* **2005,** *233* (1), 90-99.
19. Quadrelli, E. A.; Basset, J.-M., On silsesquioxanes' accuracy as molecular models for silica-grafted complexes in heterogeneous catalysis. *Coordination Chemistry Reviews* **2010,** *254* (5-6), 707-728.
20. Das, U.; Zhang, G. H.; Hu, B.; Hock, A. S.; Redfern, P. C.; Miller, J. T.; Curtiss, L. A., Effect of Siloxane Ring Strain and Cation Charge Density on the Formation of Coordinately Unsaturated Metal Sites on Silica: Insights from Density Functional Theory (DFT) Studies. *ACS Catalysis* **2015,** *5* (12), 7177-7185.
21. Guillo, P.; Lipschutz, M. I.; Fasulo, M. E.; Tilley, T. D., Tantalum–Polyhedral Oligosilsesquioxane Complexes as Structural Models and Functional Catalysts for Epoxidation. *ACS Catalysis* **2017,** *7* (4), 2303-2312.
22. Serebrinsky, S. A., Physical time scale in kinetic Monte Carlo simulations of continuous-time Markov chains. *Phys Rev E Stat Nonlin Soft Matter Phys* **2011,** *83* (3 Pt 2), 037701.
23. Andersen, M.; Panosetti, C.; Reuter, K., A Practical Guide to Surface Kinetic Monte Carlo Simulations. *Front Chem* **2019,** *7*, 202.
24. Prats, H.; Posada-Pérez, S.; Rodriguez, J. A.; Sayós, R.; Illas, F., Kinetic Monte Carlo Simulations Unveil Synergic Effects at Work on Bifunctional Catalysts. *ACS Catalysis* **2019,** *9* (10), 9117-9126.
25. Sohn, H.; Camacho-Bunquin, J.; Langeslay, R. R.; Ignacio-de Leon, P. A.; Niklas, J.; Poluektov, O. G.; Liu, C.; Connell, J. G.; Yang, D.; Kropf, J.; Kim, H.; Stair, P. C.; Ferrandon, M.; Delferro, M., Isolated, well-defined organovanadium(iii) on silica: single-site catalyst for hydrogenation of alkenes and alkynes. *Chemical Communications* **2017,** *53* (53), 7325-7328.
26. Kaphan, D. M.; Ferrandon, M. S.; Langeslay, R. R.; Celik, G.; Wegener, E. C.; Liu, C.; Niklas, J.; Poluektov, O. G.; Delferro, M., Mechanistic Aspects of a Surface Organovanadium(III) Catalyst for Hydrocarbon Hydrogenation and Dehydrogenation. *ACS Catal* **2019,** *9* (12), 11055-11066.
27. Frisch, M. J.; Trucks, G. W.; Schlegel, H. B.; Scuseria, G. E.; Robb, M. A.; Cheeseman, J. R.; Scalmani, G.; Barone, V.; Petersson, G. A.; Nakatsuji, H.; Li, X.; Caricato, M.; Marenich, A. V.; Bloino, J.; Janesko, B. G.; Gomperts, R.; Mennucci, B.; Hratchian, H. P.; Ortiz, J. V.; Izmaylov, A. F.; Sonnenberg, J. L.; Williams; Ding, F.; Lipparini, F.; Egidi, F.; Goings, J.; Peng, B.; Petrone, A.; Henderson, T.; Ranasinghe, D.; Zakrzewski, V. G.; Gao, J.; Rega, N.; Zheng, G.; Liang, W.; Hada, M.; Ehara, M.; Toyota, K.; Fukuda, R.; Hasegawa, J.; Ishida, M.; Nakajima, T.; Honda, Y.; Kitao, O.; Nakai, H.; Vreven, T.; Throssell, K.; Montgomery Jr., J. A.; Peralta, J. E.; Ogliaro, F.; Bearpark, M. J.; Heyd, J. J.; Brothers, E. N.; Kudin, K. N.; Staroverov, V. N.; Keith, T. A.; Kobayashi, R.; Normand, J.; Raghavachari, K.; Rendell, A. P.; Burant, J. C.; Iyengar, S. S.; Tomasi, J.; Cossi, M.; Millam, J. M.; Klene, M.; Adamo, C.; Cammi, R.; Ochterski, J. W.; Martin, R. L.; Morokuma, K.; Farkas, O.; Foresman, J. B.; Fox, D. J. *Gaussian 16 Rev. C.01*, Wallingford, CT, 2016.
28. Becke, A. D., Density-functional thermochemistry. III. The role of exact exchange. *Journal of Chemical Physics* **1993,** *98*, 5648-5652.
29. Lee, C.; Yang, W.; Parr, R. G., Development of the Colle-Salvetti correlation-energy formula into a functional of the electron density. *Physical Review B: Condensed Matter* **1988,** *37* (2), 785-789.

30. Stevens, W. J.; Basch, H.; Krauss, M., Compact effective potentials and efficient shared-exponent basis sets for the first- and second-row atoms. *Journal of Chemical Physics* **1984,** *81* (12), 6026-6033.
31. Stevens, W. J.; Krauss, M.; Basch, H.; Jasien, P. G., Relativistic compact effective potentials and efficient, shared-exponent basis sets for the third-, fourth-, and fifth-row atoms. *Canadian Journal of Chemistry* **1992,** *70* (2), 612-630.
32. Cundari, T. R.; Stevens, W. J., Effective core potential methods for the lanthanides. *Journal of Chemical Physics* **1993,** *98*, 5555-5565.
33. Schäfer, A.; Huber, C.; Ahlrichs, R., Fully optimized contracted Gaussian basis sets of triple zeta valence quality for atoms Li to Kr. *Journal of Chemical Physics* **1994,** *100* (8), 5829-5835.
34. Rataboul, F.; Baudouin, A.; Thieuleux, C.; Veyre, L.; Coperet, C.; Thivolle-Cazat, J.; Basset, J. M.; Lesage, A.; Emsley, L., Molecular understanding of the formation of surface zirconium hydrides upon thermal treatment under hydrogen of [([triple bond]SiO)Zr(CH2tBu)3] by using advanced solid-state NMR techniques. *J Am Chem Soc* **2004,** *126* (39), 12541-50.

TOC Image

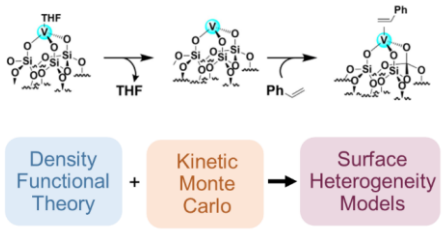

Density Functional Theory + Kinetic Monte Carlo → Surface Heterogeneity Models